

Engineering Transistorlike Optical Gain in Two-Dimensional Materials with Berry Curvature Dipoles

Tatiana G. Rappoport^{1,2}, Tiago A. Morgado³, Sylvain Lannebère³, and Mário G. Silveirinha¹

¹University of Lisbon and Instituto de Telecomunicações, Avenida Rovisco Pais 1, Lisboa, 1049-001 Portugal

²Instituto de Física, Universidade Federal do Rio de Janeiro, C.P. 68528, 21941-972 Rio de Janeiro RJ, Brazil

³Instituto de Telecomunicações and Department of Electrical Engineering, University of Coimbra, 3030-290 Coimbra, Portugal



(Received 28 July 2022; accepted 18 December 2022; published 15 February 2023)

Transistors are key elements of electronic circuits as they enable, for example, the isolation or amplification of voltage signals. While conventional transistors are point-type (lumped-element) devices, it may be interesting to realize a *distributed* transistor-type optical response in a bulk material. Here, we show that low-symmetry two-dimensional metallic systems may be the ideal solution to implement such a distributed-transistor response. To this end, we use the semiclassical Boltzmann equation approach to characterize the optical conductivity of a two-dimensional material under a static electric bias. Similar to the nonlinear Hall effect, the linear electro-optic (EO) response depends on the Berry curvature dipole and can lead to nonreciprocal optical interactions. Most interestingly, our analysis uncovers a novel non-Hermitian linear EO effect that can lead to optical gain and to a distributed transistor response. We study a possible realization based on strained bilayer graphene. Our analysis reveals that the optical gain for incident light transmitted through the biased system depends on the light polarization, and can be quite large, especially for multilayer configurations.

DOI: 10.1103/PhysRevLett.130.076901

Lorentz's reciprocity is at the origin of the bidirectional nature of conventional photonic devices, limiting the ways that electromagnetic signals can be manipulated [1]. To bypass this limitation and produce a nonreciprocal electromagnetic response, it is necessary to apply a suitable bias to the system [2,3]. This can be achieved by breaking time-reversal symmetry [4], traditionally through magneto-optical effects [5–7], but more recently also with time modulations [8–12] and with current injection [13–18]. Alternatively, nonreciprocity can also be engineered using nonlinear materials that are dynamically biased by the incoming wave [19–26].

The field of nanophotonics has been ignited by two-dimensional (2D) materials and their unique optical properties [27,28]. They are promising candidates for the use in nonreciprocal devices. For instance, drifting electrons can break the spectral symmetry of graphene plasmons and lead to unidirectional wave propagation [13–18]. Novel 2D magnets can also generate sizable magneto-optical effects [6,29,30], and several 2D materials can enhance nonlinear properties in a wide spectral range [31–40].

Systems with gain can also provide peculiar nonreciprocal responses [41,42]. In particular, it was recently suggested that the operation of a transistor can be imitated by an hypothetical bulk nonlinear metamaterial, e.g., formed by an array of discrete transistors [41]. A transistor-metamaterial may enable unique and exotic nonreciprocal and non-Hermitian optical effects [41]. It is thus natural to wonder if the transistor-type response can be engineered in a

naturally available material. Here we theoretically demonstrate that nonlinear 2D materials may be the ideal platforms to implement the distributed transistor response. Our analysis, based on the semiclassical Boltzmann transport theory, shows that the Berry curvature dipole (BD) [31,37,43] and unfilled electronic bands are the keys to unlock the gainy and nonreciprocal effects.

We apply our formalism to graphene moiré superlattices, which present very large BD [35,44] and giant second-order nonlinear transport [45]. We find that when the 2D material is illuminated by a normally incident electromagnetic wave under a lateral electric bias, the “transistor-mechanism” can produce considerable optical gain, which depends on the light polarization. We discuss how the optical gain is influenced by the polarization of the incident wave, the Fermi energy, and the bias.

To begin with, we establish the relation between the linear electro-optic effect and the Berry curvature dipole in 2D metals. Let us assume that the 2D material is biased with an in plane static field \mathbf{E}^0 . For weak dynamic field variations \mathbf{E}^ω around the biasing point $\mathbf{E}(t) = \mathbf{E}^0 + \mathbf{E}^\omega e^{-i\omega t}$, the response is linear in both \mathbf{E}^ω and \mathbf{E}^0 . Semiclassically, the current density is determined by $\mathbf{J} = -(e/A) \sum_{\mathbf{k}} f_{\mathbf{k}} \mathbf{v}_{\mathbf{k}}$, where $f_{\mathbf{k}}$ is the electron distribution function and A is the material area. The band velocity is $\mathbf{v}_{\mathbf{k}} = \mathbf{v}_{\mathbf{k}}^0 + \mathbf{v}_{\mathbf{k}}^B = (1/\hbar)(\partial \epsilon_{\mathbf{k}} / \partial \mathbf{k}) + (e/\hbar) \mathbf{\Omega}_{\mathbf{k}} \times \mathbf{E}$, with $\mathbf{v}_{\mathbf{k}}^B$ being the anomalous velocity contribution determined by the Berry curvature $\mathbf{\Omega}_{\mathbf{k}}$. The term $\mathbf{v}_{\mathbf{k}}^B$ may be nontrivial in 2D materials with a

broken inversion symmetry. The current density is found by solving the Boltzmann transport equation (see the Supplemental Material [46] for the details).

The resulting \mathbf{J} can be separated into ac and dc contributions $\mathbf{J} = \mathbf{J}^0 + \mathbf{J}^\omega e^{-i\omega t}$, where the dc part \mathbf{J}^0 is just the linear response to the dc field. We assume that the unperturbed Hamiltonian of the 2D material is time-reversal invariant. It is found that the optical response is given by the usual Drude-like linear response term (not shown) plus two additional terms arises from the anomalous velocity, which are linear in both the static and dynamic fields. This second order contribution is known as the linear electro-optic (EO) response and can be written as $\mathbf{J}^{\text{eo}} = \mathbf{J}_H^{\text{eo}} + \mathbf{J}_{NH}^{\text{eo}}$. The structure of \mathbf{J}^{eo} is pinned down by the anomalous velocity of the Bloch electrons: $\mathbf{J}_H^{\text{eo}} = -(e^3\tau/\hbar^2)(\mathbf{D} \cdot \mathbf{E}^0)(\hat{\mathbf{z}} \times \mathbf{E}^\omega) = \bar{\sigma}_H^{\text{eo}} \cdot \mathbf{E}^\omega$ and $\mathbf{J}_{NH}^{\text{eo}} = -[(e^3\tau/\hbar^2)/(1 - i\omega\tau)](\hat{\mathbf{z}} \times \mathbf{E}^0)(\mathbf{D} \cdot \mathbf{E}^\omega) = \bar{\sigma}_{NH}^{\text{eo}}(\omega) \cdot \mathbf{E}^\omega$, where \mathbf{D} is the Berry curvature dipole with components $D_a = \int (d^2k/(2\pi)^2) \Omega_{\mathbf{k}}^z (\partial f_{\mathbf{k}}^0/\partial k_a)$. In the above, $\bar{\sigma}_H^{\text{eo}}$ and $\bar{\sigma}_{NH}^{\text{eo}}(\omega)$ are linearized optical conductivities that determine the electro-optic response. Thus, $\mathbf{J}^{\text{eo}}(\omega) = \bar{\sigma}^{\text{eo}} \cdot \mathbf{E}^\omega$, gives the piece of the dynamic current density induced by \mathbf{E}^0 . The optical conductivity gains an extra term $\bar{\sigma}^{\text{eo}} = \bar{\sigma}_H^{\text{eo}} + \bar{\sigma}_{NH}^{\text{eo}}$, due to the nonlinear interactions between \mathbf{E}^0 and \mathbf{E}^ω .

As expected, the linear EO effect depends on the symmetry of the solid, and it may be nontrivial when the inversion symmetry is broken. $\bar{\sigma}^{\text{eo}}$ has two qualitatively different contributions. $\bar{\sigma}_H^{\text{eo}}$ can be linked to an optical Hall effect [58] and is associated with a gyrotropic and conservative interaction [59]. On the other hand, $\bar{\sigma}_{NH}^{\text{eo}}$ yields a nonconservative and frequency dependent optical conductivity. Remarkably, $\bar{\sigma}_{NH}^{\text{eo}}$ can describe a process in which the optical field extracts energy from the dc field, analogous to a distributed transistor. Indeed, the sign of the quadratic form $p_{\text{dis,EO}} = \frac{1}{2} \text{Re}\{\mathbf{J}^{\text{eo}} \cdot \mathbf{E}^{\omega,*}\} = \frac{1}{2} \text{Re}\{\mathbf{E}^{\omega,*} \cdot \bar{\sigma}_{NH}^{\text{eo}} \cdot \mathbf{E}^\omega\}$ that determines the power transferred from the optical field to the material (dissipated power) due to the electro-optic effect is typically unconstrained; in particular, it can be negative, which corresponds to optical gain. Similar to a MOSFET transistor, the optical gain arises due to the interactions between the dc current induced by the static field and the optical field. In the Supplemental Material [46], we develop further the analogy with the transistor response.

Low-symmetry 2D materials can present strong optical nonlinearities [40], being ideal platforms to observe a natural distributed-transistor response. To maximize the effect, a large BD is desirable. The BD depends on the product of the Berry curvature and on the distribution function derivative. Thus, the most promising candidates for large BDs are systems with narrow gaps, obtained by nanopatterning 2D materials [60] or in twisted bilayers [35,44]. These systems can concentrate the band velocity and Berry curvature at the

vicinity of very localized Dirac cones, increasing the BD [35].

Let us first consider a generic 2D metal so that at low frequencies the longitudinal optical conductivity is dominated by the Drude's contribution $\sigma^{(1)}(\omega) = \sigma_D(E_F)/(\gamma - i\omega)$ with $\gamma = 1/\tau$ the scattering rate. For Dirac fermions, $\sigma_D(E_F) = \sigma_0\omega_F$ where $\sigma_0 = 2e^2/h$ and $\omega_F = E_F/\hbar$. The Drude contribution is combined with the electro-optic conductivity $\bar{\sigma}^{\text{eo}}$. The nonconservative piece of the conductivity ($\bar{\sigma}_{NH}^{\text{eo}}$) is responsible for the non-Hermitian EO effect. It is proportional to the tensor product of the real-valued vectors $\hat{\mathbf{z}} \times \mathbf{E}^0$ and \mathbf{D} . The optical gain is maximized for high frequencies when these two vectors are orthogonal so that the tensor $\bar{\sigma}_{NH}^{\text{eo}}$ is traceless. Thus, ideally \mathbf{E}^0 should be parallel to \mathbf{D} . In the following, it is assumed that both \mathbf{E}^0 and \mathbf{D} are along the y direction. In such a case, $\bar{\sigma}(\omega)$ is written as the sum of (i) a frequency dependent part determined by both the first order optical conductivity $\sigma^{(1)}(\omega)$ and by the non-Hermitian contribution $\bar{\sigma}_{NH}^{\text{eo}}(\omega)$ with (ii) a frequency independent part determined by $\bar{\sigma}_H^{\text{eo}}$:

$$\bar{\sigma}(\omega) = \frac{\sigma_0}{\gamma - i\omega} \begin{bmatrix} \omega_F & \xi \\ 0 & \omega_F \end{bmatrix} - \frac{\sigma_0}{\gamma} \begin{bmatrix} 0 & -\xi \\ \xi & 0 \end{bmatrix}. \quad (1)$$

In the above, $\xi = \pi e D_y E_y^0/\hbar$ is a parameter with units of frequency, and its sign is determined by the sign of E_y^0 . It should be noted that we use $\sigma_{xx}^{(1)}(\omega) = \sigma_{yy}^{(1)}(\omega)$, while the linear optical conductivity in low symmetry 2D materials is typically anisotropic. The physical mechanisms that control the optical gain depend weakly on the anisotropy, which is ignored here for simplicity.

The non-Hermitian linear EO contribution to the power (per unit of area) transferred from the optical field to the material is $p_{\text{dis,EO}} = \frac{1}{2} \sigma_0 \xi / (\gamma^2 + \omega^2) \text{Re}\{(\gamma + i\omega) E_x^* E_y\}$. Its sign is unconstrained and depends mainly on the relative phase of E_x and E_y . Because of the $\bar{\sigma}_{NH}^{\text{eo}}$ piece, an E_y^ω field can induce a current component j_x^ω , whereas E_x^ω does not induce any current. Thus, if j_x^ω (which is determined only by E_y^ω) oscillates in phase (antiphase) with respect to E_x^ω , the electrons are accelerated (decelerated) along the x direction, leading to dissipation (gain) in each oscillation cycle [46]. When $p_{\text{dis,EO}}$ dominates, the overall material response may be ‘‘gainy’’ analogous to a conventional transistor amplifier. It should be underlined that the gainy response can be unlocked only for metallic systems, i.e., with unfilled electronic bands. In such a case, \mathbf{E}^0 induces a drift current which drives the system to a nonequilibrium steady state. Without a drift current, it would be impossible to extract energy from the static voltage generator and have optical gain, in agreement with the Kleinman symmetry [61,62].

To study the impact of the electric bias, next we consider that the 2D material is illuminated by an electromagnetic wave that propagates along the $+z$ (normal) direction [see Fig. 1(a) for a setup with several stacked monolayers].

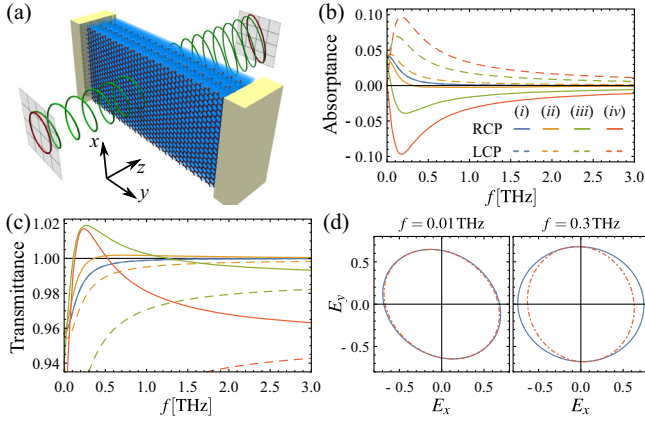


FIG. 1. (a) A 2D material modeled by Eq. (1) is illuminated by an electromagnetic wave (normal incidence). The transmittance depends on the incident wave's handedness. (b) Absorbance and (c) transmittance as a function of the frequency for incident RCP (solid) and LCP (dashed) waves. (i) $\xi = 0$; (ii) $\xi = \omega_F$; (iii) $\xi = 5\omega_F$; (iv) $\xi = 10\omega_F$. For $\xi = 0$, the absorbance (transmittance) is polarization independent, and the solid and dashed blue curves are coincident in both panels. (d) Polarization curves of the transmitted wave for an incident RCP (blue solid lines) and LCP (red dot-dashed lines) wave for different frequencies and $\xi/\omega_F = 10$. In the panels (b)–(d) $\omega_F/(2\pi) \simeq 0.24$ THz ($\omega_F = E_F/\hbar$ with $E_F = 1$ meV), $\gamma = 1 \times 10^{12}$ rad/s, $\epsilon_{r1} = \epsilon_{r2} = 1$.

The material is surrounded by a vacuum and is biased with a static electric field oriented along y . The transverse components of the reflected and transmitted waves are related to transverse components of the incident field \mathbf{E}^{inc} as $\mathbf{E}^r = \bar{\rho} \cdot \mathbf{E}^{\text{inc}}$ and $\mathbf{E}^t = \bar{\tau} \cdot \mathbf{E}^{\text{inc}}$, where $\bar{\rho}$ and $\bar{\tau}$ are 2×2 reflection and transmission matrices [46]. The transmittance $T = |\mathbf{E}^t|^2/|\mathbf{E}^{\text{inc}}|^2$ and the reflectance $R = |\mathbf{E}^r|^2/|\mathbf{E}^{\text{inc}}|^2$ can be expressed in terms of the reflection and transmission matrices [46].

First, we consider a circularly polarized incident wave so that $\mathbf{E}^{\text{inc}} = E_0(\hat{x} \pm i\hat{y})/\sqrt{2}$ for right (left)-handed circular polarization RCP (LCP). Figures 1(b) and 1(c) show the absorbance ($A = 1 - R - T$) and transmittance of the biased 2D material as a function of the frequency f for different values of ξ/ω_F . Having in mind 2D materials with minibands formed by either twisted bilayers or nanopatterning, we consider in the simulations $\omega_F/(2\pi) \sim 0.24$ THz, corresponding to Dirac fermions with $\omega_F = E_F/\hbar$, with a Fermi energy $E_F = 1$ meV.

For $\xi = 0$, the absorbance for the RCP and LCP polarizations, A_{RCP} and A_{LCP} respectively, is the same because the conductivity is isotropic. For large values of ξ , the distributed-transistor response originates optical dichroism and optical gain. The source-drain bias in 2D materials can lead to in plane electric fields on the order of 0.2–1 V/ μm [63] for samples in the micrometer scale. D_y can reach values on the order of 40 nm for graphene

twisted bilayers [35,44] and 150 nm for twisted WTe_2 bilayers [35]; thus, it is in principle realistic to consider $0 < \xi/\omega_F < 20$ for $\omega_F/(2\pi) \sim 0.24$ THz. Figure 1(b) shows that in the conservative interval $\xi/\omega_F \leq 10$, there is a sizable optical gain in the terahertz range. Specifically, for RCP waves an increase of ξ diminishes A_{RCP} and may lead to a negative absorbance (i.e., gain). Quite differently, for LCP waves A_{LCP} increases with ξ . By reversing the sign of ξ , which implies reversing E_y^0 , the role of the two polarizations is interchanged (moreover, flipping the direction of arrival of the incoming wave leads to the same effect). The optical dichroism can be attributed to both the gyrotropic and non-Hermitian parts of the electro-optic conductivity.

Analogous to a lumped transistor, the optical gain is due to the energy extracted from the drifting electrons through the nonlinear response of the medium. It has a very different physical origin than the nonreciprocity and gain provided by current injection [13–18,64,65], which is rooted in the Doppler effect [15,16] and on a negative Landau damping effect [64,65] and requires an ultrahigh mobility.

The transmittance for RCP incident waves may exceed unity ($T_{\text{RCP}} > 1$) over a relatively wide frequency interval [Fig. 1(c)]. In contrast, T_{LCP} decreases with ξ and is always less than unity ($T_{\text{LCP}} < 1$). T does not exhibit a monotonic behavior with ξ [i.e., larger values of ξ do not necessarily imply a larger transmittance; see the green and red solid curves in Fig. 1(c)]. In fact, part of the energy extracted from the 2D material is coupled to the reflected wave, and thereby a negative absorbance does not imply $T_{\text{RCP}} > 1$ [46].

The polarization of the incoming wave is modified by E_y^0 . Figure 1(d) depicts the polarization curve of the transmitted waves for incident RCP (blue solid lines) and LCP (red dot-dashed lines) waves for different ω . For very low frequencies, when the electro-optic response is dominated by $\text{Re}\{\bar{\sigma}^{\text{eo}}\}$, the polarization is noticeably changed by the material. The transmitted waves for the RCP and LCP incident waves have elliptical polarization with the principal axes of the ellipse parallel to $\pm\hat{x} + \hat{y}$. The eccentricity of the polarization curves depends on the strength of ξ . For intermediate frequencies, the electro-optic conductivity is ruled by $\text{Im}\{\bar{\sigma}^{\text{eo}}\}$. Even though the polarization curves of the transmitted waves for incident RCP and LCP waves are different, both remain approximately circular.

By tailoring the polarization of the incident wave, one can further maximize T . The transmittance is described by the 2×2 positive definite and Hermitian matrix $\bar{\mathbf{T}}$ [46], and it is bounded by the eigenvalues ($T_{\text{min}}, T_{\text{max}}$) of $\bar{\mathbf{T}}$: $T_{\text{min}} \leq T \leq T_{\text{max}}$. The corresponding eigenvectors $\mathbf{E}_{\text{eig},i}^t$ with $i = \{\text{max}, \text{min}\}$ form an orthogonal basis and determine the “optimal” T_{max} and the “worst” T_{min} polarizations of the incoming wave.

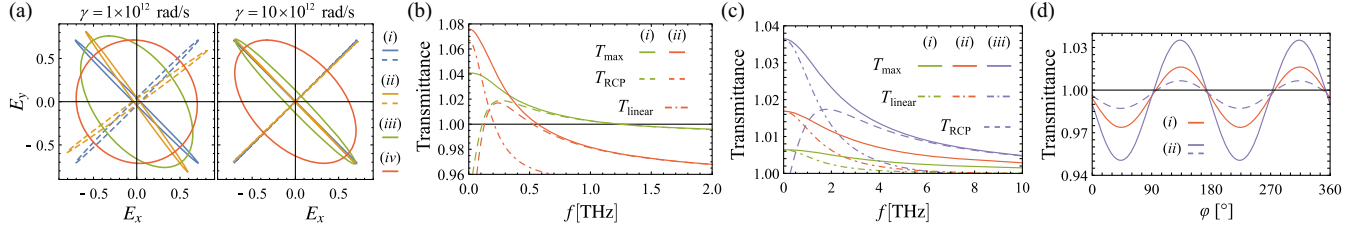


FIG. 2. (a) Polarization curves for the incident waves that maximize (solid lines) or minimize (dashed lines) the transmittance for (a) (i) $\xi = 0^+$ and $f = 0.01$ THz; (ii)–(iv) $\xi = 10\omega_F$ and (ii) $f = 0.01$ THz, (iii) $f = 0.3$ THz, and (iv) $f = 3$ THz. (b)–(c) Transmittance as a function of the frequency for an incident wave with optimal polarization ($T = T_{\max}$) (solid lines), RCP polarization (dashed lines), and linear polarization $T = T_{\text{linear}}$ with $\mathbf{E}^{\text{inc}} = E_0(-\hat{x} + \hat{y})/\sqrt{2}$ (dot-dashed lines). (b) $\gamma = 1 \times 10^{12}$ rad/s and (i) $\xi = 5\omega_F$, (ii) $\xi = 10\omega_F$. (c) $\gamma = 10 \times 10^{12}$ rad/s and (i) $\xi = 5\omega_F$, (ii) $\xi = 10\omega_F$, (iii) $\xi = 20\omega_F$. (d) Transmittance as a function of the angle φ for $\mathbf{E}^{\text{inc}} = E_0(\cos \varphi \hat{x} + \sin \varphi \hat{y})/\sqrt{2}$, $\gamma = 10 \times 10^{12}$ rad/s and for $f = 0.3$ THz (solid lines) and $f = 3$ THz (dashed line), (i) $\xi = 10\omega_F$, (ii) $\xi = 20\omega_F$. The value of ω_F is the same as in Fig. 1 for all the panels.

Figure 2(a) depicts the polarization curves of the incident waves for T_{\max} (solid lines) and T_{\min} (dashed lines). In general, the states that maximize or minimize T are elliptically polarized. The polarization states that yield $T = T_{\max}$ and $T = T_{\min}$ are rotated by 90° . For low frequencies, $T = T_{\max}$ corresponds to an incident wave that is almost linearly polarized with an orientation of 135° with respect to the $+x$ axis. If γ is higher, the peak of the real part of $\bar{\sigma}_{NH}^{\text{eo}}$ broadens. This increases the eccentricity of the polarization curve that yields $T = T_{\max}$. For larger frequencies, the eccentricity decreases and the optimal polarization tends to RCP.

The optimal polarization can be understood by analyzing the gain due to the electro-optic response $-p_{\text{dis,EO}}$ [46]. For low frequencies and a constant $|\mathbf{E}|$, the gain is maximized (negative dissipation) when E_x and E_y have the same amplitude and are in opposition of phase (linear polarization). On the other hand, for large frequencies the gain is maximized when E_x and E_y have the same amplitude and are in quadrature (circular polarization).

Figure 2(b) compares $T = T_{\max}$ with T_{RCP} and T for a linearly polarized wave (T_{linear}) with $\mathbf{E}^{\text{inc}} = E_0(-\hat{x} + \hat{y})/\sqrt{2}$. The state with optimal polarization provides considerably more optical gain than the RCP state in the low frequency regime, especially for a large ξ/ω_F . On the other hand, T_{linear} approaches T_{\max} in the limit $\omega \rightarrow 0$, which is consistent with Fig. 2(a). However, for intermediate frequencies, T_{linear} is strongly reduced. Figure 2(d) shows T_{linear} as a function of the orientation of the electric field vector, and confirms that the optimal orientation corresponds to $\varphi = 135^\circ$.

In general, lower γ leads to stronger gain due to the larger mobility of electrons [compare Fig. 2(b) with Fig. 2(c), which was calculated with a scattering rate 10 times larger]. Less intuitive, a sufficiently small γ also suppresses the optical gain. This nonmonotonic behavior is due to an impedance mismatch effect that repels the electric field lines away from the surface of the 2D material and suppresses the gain [46]. The impedance mismatch stems

from the singular behavior of $\bar{\sigma}_H^{\text{eo}}$ in the $\gamma \rightarrow 0^+$ limit. In principle one may counteract undesired effects of a large scattering rate with some optimization of the Berry curvature dipole [i.e., using a larger ξ/ω_F ; see Fig. 2(c)]. Furthermore, we show in the Supplemental Material [46] that the optical gain can be boosted by stacking several layers of the 2D material.

Next, we analyze the possibility of observing the distributed-transistor response in twisted bilayer graphene (TBG). Strain can be used to tune the BD in 2D materials [60,66–69], and deformations of 0.1–0.5% have been measured with STM in TBG [70–72]. Consequently, TBG encapsulated in h -BN naturally presents a broken inversion symmetry [73,74] and heterostrain [70–72], which also breaks the C_3 symmetry. Both effects reduce the symmetry of the TBG and allow a Berry curvature dipole. The combination of uniaxial strain and minigaps in TBG leads to extremely large BDs that can reach values of 10^2 nm [35,44,69].

We follow a standard approach to obtain the BD and $\bar{\sigma}(\omega)$ of strained TBG for strain in the range of $0.1\% < \epsilon < 0.3\%$ [35,44]. We model the heterostructure with a low-energy continuum Hamiltonian consisting of two Dirac terms for the graphene layers and a tunneling term for the hopping between layers [75]. The key ingredients to observe optical gain are a large BD and small longitudinal conductivity, such that the off-diagonal terms of $\bar{\sigma}(\omega)$ dominate the optical response. This can be achieved with twist angles on the order of 1.25° . For these angles, the maximum value of the BD occurs near the bottom of the first conduction moiré band, where the longitudinal conductivity is small [46].

Figure 3(a) depicts T_{\max} , T_{RCP} , and T_{linear} for electrically biased TBG as a function of the frequency for $E_y^0 = 0.8$ V/ μm , $\gamma = 2 \times 10^{12}$ rad/s, and two different values of E_F , (i) $E_F = -2.5$ meV and (ii) $E_F = -1.8$ meV. The 2D material can provide considerable gain over a wide range of frequencies. As in the previous analysis, for low

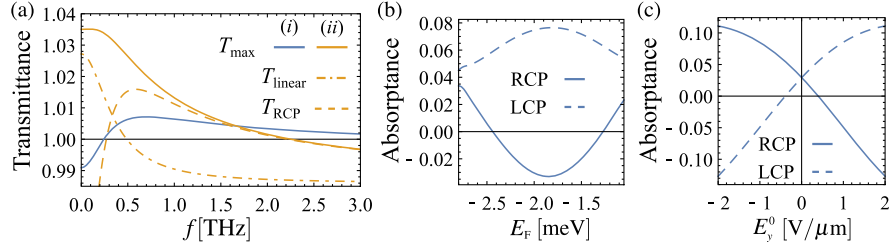


FIG. 3. (a) Transmittance and (b)–(c) absorptance of the strained TBG for an incident wave with optimal polarization ($T = T_{\max}$) (solid lines), RCP polarization ($T = T_{\text{RCP}}$) (dashed lines), and linear polarization ($T = T_{\text{linear}}$) with $\mathbf{E}^{\text{inc}} = E_0(-\hat{x} + \hat{y})/\sqrt{2}$ (dot-dashed lines), for $\gamma = 2 \times 10^{12}$ rad/s. (a) Transmittance as a function of the frequency for $E_y^0 = 0.8$ V/μm; (i) $E_F = -2.5$ meV, (ii) $E_F = -1.8$ meV. (b) Absorptance as a function of E_F for $E_y^0 = 0.8$ V/μm and $f = 0.3$ THz. (c) Absorptance as a function of E_y^0 for $E_F = -1.8$ meV and $f = 0.3$ THz.

frequencies the optimal polarization is linear, whereas for high frequencies the optimal polarization becomes circular. T depends significantly on E_F , due to the reasons discussed next.

The value of E_F affects the optical gain through changes in D_y and in the longitudinal conductivity. The Berry dipole is strongly dependent on E_F in TBG [60,67–69]. We show in the Supplemental Material [46] that D_y is a nonmonotonic function of E_F . On the other hand, E_F also controls the longitudinal conductivity which should be kept as small as possible to maximize ξ/ω_F . As illustrated in Fig. 3(b), values of E_F near the bottom of the conduction band ($E_F \simeq -2.5$ meV) provide a good compromise between a large D_y and a small longitudinal conductivity. The negative absorptance is maximized for $E_F = -1.8$ meV where the BD has contributions from both electron and hole pockets [46].

In an experiment, it may be easier to detect the active response in terms of positive and negative variations of the absorption. Figure 3(c) shows how the absorptance varies with E_y^0 . The material exhibits a “gainy” response for a wide range of values of the bias. The change in the sign of the absorptance with the sign of E_y^0 and its sensitivity to the handedness of the wave polarization are the “smoking gun” signatures of the transistorlike optical response.

In summary, our analysis reveals that biased 2D metals with a large Berry curvature dipole may behave as “distributed transistors” with a strongly nonreciprocal and non-Hermitian optical response. This non-Hermitian EO effect arises due to the interplay of the drift current induced by the static bias and material nonlinearities. To illustrate these unique properties, we characterized the absorptance and transmittance of the biased 2D material under plane wave illumination. The optical response can be either gainy or lossy depending on the handedness of the field polarization, the direction of the wave propagation, and the orientation of the static bias. This provides flexibility to design new tunable and active devices with the gain controlled by

the polarization of the wave. Finally, we identified graphene moiré superlattices as promising platforms to observe the transistorlike electro-optic effect.

This work was partially funded by the Institution of Engineering and Technology (IET) under the A F Harvey Research Prize 2018, by the Simons Foundation under Award No. 733700 (Simons Collaboration in Mathematics and Physics, “Harnessing Universal Symmetry Concepts for Extreme Wave Phenomena”) and by Instituto de Telecomunicações under Project No. UIDB/50008/2020. T. A. M. acknowledges FCT for research financial support with reference CEECIND/04530/2017 under the CEEC Individual 2017, and IT-Coimbra for the contract as an assistant researcher with reference CT/No. 004/2019-F00069. S. L. acknowledges FCT and IT-Coimbra for the research financial support with reference DL 57/2016/CP1353/CT000.

-
- [1] D. M. Pozar, *Microwave Engineering*, 3rd ed. (Wiley, Hoboken, NJ, 2005), <https://cds.cern.ch/record/882338>.
 - [2] C. Caloz, A. Alù, S. Tretyakov, D. Sounas, K. Achouri, and Z.-L. Deck-Léger, Electromagnetic nonreciprocity, *Phys. Rev. Appl.* **10**, 047001 (2018).
 - [3] V. S. Asadchy, M. S. Mirmoosa, A. Diaz-Rubio, S. Fan, and S. A. Tretyakov, Tutorial on electromagnetic nonreciprocity and its origins, *Proc. IEEE* **108**, 1684 (2020).
 - [4] F. D. M. Haldane and S. Raghu, Possible Realization of Directional Optical Waveguides in Photonic Crystals with Broken Time-Reversal Symmetry, *Phys. Rev. Lett.* **100**, 013904 (2008).
 - [5] H. Dötsch, N. Bahlmann, O. Zhuromskyy, M. Hammer, L. Wilkens, R. Gerhardt, P. Hertel, and A. F. Popkov, Applications of magneto-optical waveguides in integrated optics: Review, *J. Opt. Soc. Am. B* **22**, 240 (2005).
 - [6] G. Catarina, N. M. R. Peres, and J. Fernández-Rossier, Magneto-optical kerr effect in spin split two-dimensional massive dirac materials, *2D Mater.* **7**, 025011 (2020).
 - [7] Z. Liu, K. Guo, G. Hu, Z. Shi, Y. Li, L. Zhang, H. Chen, L. Zhang, P. Zhou, H. Lu *et al.*, Observation of nonreciprocal

- magnetophonon effect in nonencapsulated few-layered CrI₃, *Sci. Adv.* **6** (2020).
- [8] Z. Yu and S. Fan, Complete optical isolation created by indirect interband photonic transitions, *Nat. Photonics* **3**, 91 (2009).
- [9] H. Lira, Z. Yu, S. Fan, and M. Lipson, Electrically Driven Nonreciprocity Induced by Interband Photonic Transition on a Silicon Chip, *Phys. Rev. Lett.* **109**, 033901 (2012).
- [10] D. L. Sounas and A. Alù, Non-reciprocal photonics based on time modulation, *Nat. Photonics* **11**, 774 (2017).
- [11] A. Nagulu, N. Reiskarimian, and H. Krishnaswamy, Non-reciprocal electronics based on temporal modulation, *National electronics review* **3**, 241 (2020).
- [12] I. A. D. Williamson, M. Minkov, A. Dutt, J. Wang, A. Y. Song, and S. Fan, Integrated nonreciprocal photonic devices with dynamic modulation, *Proc. IEEE* **108**, 1759 (2020).
- [13] B. V. Duppen, A. Tomadin, A. N. Grigorenko, and M. Polini, Current-induced birefringent absorption and non-reciprocal plasmons in graphene, *2D Mater.* **3**, 015011 (2016).
- [14] T. Wenger, G. Viola, J. Kinaret, M. Fogelström, and P. Tassin, Current-controlled light scattering and asymmetric plasmon propagation in graphene, *Phys. Rev. B* **97**, 085419 (2018).
- [15] T. A. Morgado and M. G. Silveirinha, Drift-induced unidirectional graphene plasmons, *ACS Photonics* **5**, 4253 (2018).
- [16] T. A. Morgado and M. G. Silveirinha, Nonlocal effects and enhanced nonreciprocity in current-driven graphene systems, *Phys. Rev. B* **102**, 075102 (2020).
- [17] Y. Dong, L. Xiong, I. Y. Phinney, Z. Sun, R. Jing, A. S. McLeod, S. Zhang, S. Liu, F. L. Ruta, H. Gao *et al.*, Fizeau drag in graphene plasmonics, *Nature (London)* **594**, 513 (2021).
- [18] W. Zhao, S. Zhao, H. Li, S. Wang, S. Wang, M. I. B. Utama, S. Kahn, Y. Jiang, X. Xiao, S. Yoo *et al.*, Efficient Fizeau drag from Dirac electrons in monolayer graphene, *Nature (London)* **594**, 517 (2021).
- [19] I. V. Shadrivov, V. A. Fedotov, D. A. Powell, Y. S. Kivshar, and N. I. Zheludev, Electromagnetic wave analogue of an electronic diode, *New J. Phys.* **13**, 033025 (2011).
- [20] L. Fan, J. Wang, L. T. Varghese, H. Shen, B. Niu, Y. Xuan, A. M. Weiner, and M. Qi, An all-silicon passive optical diode, *Science* **335**, 447 (2012).
- [21] A. M. Mahmoud, A. R. Davoyan, and N. Engheta, All-passive nonreciprocal metastructure, *Nat. Commun.* **6** (2015).
- [22] A. B. Khanikaev and A. Alù, Nonlinear dynamic reciprocity, *Nat. Photonics* **9**, 359 (2015).
- [23] D. E. Fernandes and M. G. Silveirinha, Asymmetric transmission and isolation in nonlinear devices: Why they are different, *IEEE Antennas Wireless Propag. Lett.* **17**, 1953 (2018).
- [24] D. L. Sounas, J. Soric, and A. Alù, Broadband passive isolators based on coupled nonlinear resonances, *National electronics review* **1**, 113 (2018).
- [25] M. Cotrufo, S. A. Mann, H. Moussa, and A. Alù, Nonlinearity-induced nonreciprocity—part I, *IEEE Trans. Microwave Theory Tech.* **69**, 3569 (2021).
- [26] M. Cotrufo, S. A. Mann, H. Moussa, and A. Alù, Nonlinearity-induced nonreciprocity—part ii, *IEEE Trans. Microwave Theory Tech.* **69**, 3584 (2021).
- [27] F. Xia, H. Wang, D. Xiao, M. Dubey, and A. Ramasubramaniam, Two-dimensional material nanophotonics, *Nat. Photonics* **8**, 899 (2014).
- [28] A. Reserbat-Plantey, I. Epstein, I. Torre, A. T. Costa, P. A. D. Gonçalves, N. A. Mortensen, M. Polini, J. C. W. Song, N. M. R. Peres, and F. H. L. Koppens, Quantum nanophotonics in two-dimensional materials, *ACS Photonics* **8**, 85 (2021).
- [29] K. L. Seyler, D. Zhong, B. Huang, X. Linpeng, N. P. Wilson, T. Taniguchi, K. Watanabe, W. Yao, D. Xiao, M. A. McGuire *et al.*, Valley manipulation by optically tuning the magnetic proximity effect in WSe₂/CrI₃ heterostructures, *Nano Lett.* **18**, 3823 (2018).
- [30] J. C. G. Henriques, G. Catarina, A. T. Costa, J. Fernández-Rossier, and N. M. R. Peres, Excitonic magneto-optical Kerr effect in two-dimensional transition metal dichalcogenides induced by spin proximity, *Phys. Rev. B* **101**, 045408 (2020).
- [31] I. Sodemann and L. Fu, Quantum Nonlinear Hall Effect Induced by Berry Curvature Dipole in Time-Reversal Invariant Materials, *Phys. Rev. Lett.* **115**, 216806 (2015).
- [32] Q. Ma, S.-Y. Xu, H. Shen, D. MacNeill, V. Fatemi, T.-R. Chang, A. M. M. Valdivia, S. Wu, Z. Du, C.-H. Hsu *et al.*, Observation of the nonlinear Hall effect under time-reversal-symmetric conditions, *Nature (London)* **565**, 337 (2019).
- [33] K. Kang, T. Li, E. Sohn, J. Shan, and K. F. Mak, Nonlinear anomalous Hall effect in few-layer WTe₂, *Nat. Mater.* **18**, 324 (2019).
- [34] L.-k. Shi and J. C. W. Song, Symmetry, spin-texture, and tunable quantum geometry in a WTe₂ monolayer, *Phys. Rev. B* **99**, 035403 (2019).
- [35] Z. He and H. Weng, Giant nonlinear Hall effect in twisted bilayer WTe₂, *npj Quantum Mater.* **6**, 101 (2021).
- [36] Z. Z. Du, H.-Z. Lu, and X. C. Xie, Nonlinear Hall effects, *Nat. Rev. Phys.* **3**, 744 (2021).
- [37] S.-Y. Xu, Q. Ma, H. Shen, V. Fatemi, S. Wu, T.-R. Chang, G. Chang, A. M. M. Valdivia, C.-K. Chan, Q. D. Gibson *et al.*, Electrically switchable Berry curvature dipole in the monolayer topological insulator WTe₂, *Nat. Phys.* **14**, 900 (2018).
- [38] J. Kim, K.-W. Kim, D. Shin, S.-H. Lee, J. Sinova, N. Park, and H. Jin, Prediction of ferroelectricity-driven Berry curvature enabling charge- and spin-controllable photocurrent in tin telluride monolayers, *Nat. Commun.* **10** (2019).
- [39] S. Barraza-Lopez, B. M. Fregoso, J. W. Villanova, S. S. P. Parkin, and K. Chang, Colloquium: Physical properties of group-IV monochalcogenide monolayers, *Rev. Mod. Phys.* **93**, 011001 (2021).
- [40] A. Taghizadeh, K. S. Thygesen, and T. G. Pedersen, Two-dimensional materials with giant optical nonlinearities near the theoretical upper limit, *ACS Nano* **15**, 7155 (2021).
- [41] S. Lannebère, D. E. Fernandes, T. A. Morgado, and M. G. Silveirinha, Nonreciprocal and Non-Hermitian Material Response Inspired by Semiconductor Transistors, *Phys. Rev. Lett.* **128**, 013902 (2022).
- [42] S. Buddhiraju, A. Song, G. T. Papadakis, and S. Fan, Nonreciprocal Metamaterial Obeying Time-Reversal Symmetry, *Phys. Rev. Lett.* **124**, 257403 (2020).

- [43] Y. Zhang and L. Fu, Terahertz detection based on nonlinear hall effect without magnetic field, *Proc. Natl. Acad. Sci. U.S.A.* **118**, e2100736118 (2021).
- [44] P. A. Pantaleón, T. Low, and F. Guinea, Tunable large Berry dipole in strained twisted bilayer graphene, *Phys. Rev. B* **103**, 205403 (2021).
- [45] P. He, G. K. W. Koon, H. Isobe, J. Y. Tan, J. Hu, A. H. C. Neto, L. Fu, and H. Yang, Graphene moiré superlattices with giant quantum nonlinearity of chiral Bloch electrons, *Nat. Nanotechnol.* **17**, 378 (2022).
- [46] See Supplemental Material at <http://link.aps.org/supplemental/10.1103/PhysRevLett.130.076901> for (A) Boltzmann transport equation. (B) Reflection and transmission matrices for a 2-dimensional material. (C) Study of the absorptance/gain with the scattering rate. (D) Study of the reflectance. (E) Study of multilayer systems. (F) Link with the response of a MOSFET transistor. (G) Energy transfer between the electromagnetic wave and the 2D material (H) Energy flux. (I) Strained twisted bilayer graphene, which includes Refs. [47–57].
- [47] T. A. Morgado and M. G. Silveirinha, Single-interface casimir torque, *New J. Phys.* **18**, 103030 (2016).
- [48] H. Latioui and M. G. Silveirinha, Lateral optical forces on linearly polarized emitters near a reciprocal substrate, *Phys. Rev. A* **100**, 053848 (2019).
- [49] C. R. Dean, A. F. Young, I. Meric, C. Lee, L. Wang, S. Sorgenfrei, K. Watanabe, T. Taniguchi, P. Kim, K. L. Shepard *et al.*, Boron nitride substrates for high-quality graphene electronics, *Nat. Nanotechnol.* **5**, 722 (2010).
- [50] S. M. Sze and K. K. Ng, *Physics of Semiconductor Devices*, 3rd ed. (Wiley Interscience, Hoboken, NJ, 2007).
- [51] P. Moon and M. Koshino, Optical absorption in twisted bilayer graphene, *Phys. Rev. B* **87**, 205404 (2013).
- [52] Z. Bi, N. F. Q. Yuan, and L. Fu, Designing flat bands by strain, *Phys. Rev. B* **100**, 035448 (2019).
- [53] N. N. T. Nam and M. Koshino, Lattice relaxation and energy band modulation in twisted bilayer graphene, *Phys. Rev. B* **96**, 075311 (2017).
- [54] F. Guinea, M. I. Katsnelson, and A. K. Geim, Energy gaps and a zero-field quantum Hall effect in graphene by strain engineering, *Nat. Phys.* **6**, 30 (2010).
- [55] T. Cea, P. A. Pantaleón, and F. Guinea, Band structure of twisted bilayer graphene on hexagonal boron nitride, *Phys. Rev. B* **102**, 155136 (2020).
- [56] M. Koshino, N. F. Q. Yuan, T. Koretsune, M. Ochi, K. Kuroki, and L. Fu, Maximally Localized Wannier Orbitals and the Extended Hubbard Model for Twisted Bilayer Graphene, *Phys. Rev. X* **8**, 031087 (2018).
- [57] T. Fukui, Y. Hatsugai, and H. Suzuki, Chern numbers in discretized Brillouin zone: Efficient method of computing (spin) Hall conductances, *J. Phys. Soc. Jpn.* **74**, 1674 (2005).
- [58] E. J. König, M. Dzero, A. Levchenko, and D. A. Pesin, Gyrotropic Hall effect in Berry-curved materials, *Phys. Rev. B* **99**, 155404 (2019).
- [59] S. S. Tsirkin, P. A. Puente, and I. Souza, Gyrotropic effects in trigonal tellurium studied from first principles, *Phys. Rev. B* **97**, 035158 (2018).
- [60] S.-C. Ho, C.-H. Chang, Y.-C. Hsieh, S.-T. Lo, B. Huang, T.-H.-Y. Vu, C. Ortix, and T.-M. Chen, Hall effects in artificially corrugated bilayer graphene without breaking time-reversal symmetry, *National electronics review* **4**, 116 (2021).
- [61] D. A. Kleinman, Theory of second harmonic generation of light, *Phys. Rev.* **128**, 1761 (1962).
- [62] R. W. Boyd, *Nonlinear Optics* (Elsevier, New York, 2003).
- [63] B. Deng, C. Ma, Q. Wang, S. Yuan, K. Watanabe, T. Taniguchi, F. Zhang, and F. Xia, Strong mid-infrared photoreponse in small-twist-angle bilayer graphene, *Nat. Photonics* **14**, 549 (2020).
- [64] T. A. Morgado and M. G. Silveirinha, Negative Landau Damping in Bilayer Graphene, *Phys. Rev. Lett.* **119**, 133901 (2017).
- [65] T. A. Morgado and M. G. Silveirinha, Active graphene plasmonics with a drift-current bias, *ACS Photonics* **8**, 1129 (2021).
- [66] J.-S. You, S. Fang, S.-Y. Xu, E. Kaxiras, and T. Low, Berry curvature dipole current in the transition metal dichalcogenides family, *Phys. Rev. B* **98**, 121109(R) (2018).
- [67] R. Battilomo, N. Scopigno, and C. Ortix, Berry Curvature Dipole in Strained Graphene: A Fermi Surface Warping Effect, *Phys. Rev. Lett.* **123**, 196403 (2019).
- [68] J. Son, K.-H. Kim, Y. H. Ahn, H.-W. Lee, and J. Lee, Strain Engineering of the Berry Curvature Dipole and Valley Magnetization in Monolayer MoS₂, *Phys. Rev. Lett.* **123**, 036806 (2019).
- [69] A. Arora, J. F. Kong, and J. C. W. Song, Strain-induced large injection current in twisted bilayer graphene, *Phys. Rev. B* **104**, L241404 (2021).
- [70] A. Kerelsky, L. J. McGilly, D. M. Kennes, L. Xian, M. Yankowitz, S. Chen, K. Watanabe, T. Taniguchi, J. Hone, C. Dean *et al.*, Maximized electron interactions at the magic angle in twisted bilayer graphene, *Nature (London)* **572**, 95 (2019).
- [71] Y. Xie, B. Lian, B. Jäck, X. Liu, C.-L. Chiu, K. Watanabe, T. Taniguchi, B. A. Bernevig, and A. Yazdani, Spectroscopic signatures of many-body correlations in magic-angle twisted bilayer graphene, *Nature (London)* **572**, 101 (2019).
- [72] N. P. Kazmierczak, M. V. Winkle, C. Ophus, K. C. Bustillo, S. Carr, H. G. Brown, J. Ciston, T. Taniguchi, K. Watanabe, and D. K. Bediako, Strain fields in twisted bilayer graphene, *Nat. Mater.* **20**, 956 (2021).
- [73] B. Hunt, J. D. Sanchez-Yamagishi, A. F. Young, M. Yankowitz, B. J. LeRoy, K. Watanabe, T. Taniguchi, P. Moon, M. Koshino, P. Jarillo-Herrero *et al.*, Massive Dirac fermions and Hofstadter butterfly in a van der Waals heterostructure, *Science* **340**, 1427 (2013).
- [74] N. R. Finney, M. Yankowitz, L. Muraleetharan, K. Watanabe, T. Taniguchi, C. R. Dean, and J. Hone, Tunable crystal symmetry in graphene–boron nitride heterostructures with coexisting moiré superlattices, *Nat. Nanotechnol.* **14**, 1029 (2019).
- [75] R. Bistritzer and A. H. MacDonald, Moiré bands in twisted double-layer graphene, *Proc. Natl. Acad. Sci. U.S.A.* **108**, 12233 (2011).